

of 1 and 2 mag attenuation. Since the example is chosen in such a way that the wings of the bright star are already close to nonlinearity, the SNR in the wings does not change dramatically with the choice of filters. The core of the bright star is therefore always beyond saturation, i.e. at zero level. Note the behaviour of the faint star. Without attenuation it is also subject to oversaturation, i.e., is represented by a hole in the wings of the bright star's image because the faint star's flux is added to this very high background. Adding stronger and stronger attenuating filters actually increases the detectability: With a 2 mag density filter in the beam, the SNR is superior to the 1 mag combination.

This last example demonstrates nicely, how much experience can be gained from mere simulations. Obviously, there will always be observations that reveal the unpredicted and therefore cannot be anticipated during simulations. What

can be learned, however, is the awareness of problems that may be unimportant under certain circumstances (which usually are not encountered by most ground-based observing programmes) but can determine completely the outcome of another type of observation.

5. Availability

The model package is available for use at the ST-ECF, ESO, Garching. On-line help facilities, a Users Guide and documentation of the Data Bases are provided. Although its main purpose is to simulate HST observations, it can easily be adapted to other instrumentations as well, and we anticipate that the instrumental data of cameras, filters and spectrographs in operation at ESO, La Silla, will become available. Prerequisites for a successful use of the model are experience with the MIDAS system, a detailed prescription of the astronomical target to be generated and familiarity

with the HST Instrument Users Guides applicable. A minimum of 3 days should be allocated for a typical project. Prospective users should contact the ST-ECF for details, arrangements of staff support and booking of computer time.

6. Acknowledgements

Besides ST-ECF staff, the following individuals and groups have contributed data, software, and discussions: K. Banse and D. Ponz (ESO Image Processing Group), members of the Instrument Support Branch and others at the STScI, in particular S. Ewald, G. Hartig and F. Paresce. D. Carr and C. Prasch were involved in most of the laborious work of extracting and editing the instrument data base, etc. from handbooks and other sources. Finally, all those colleagues who have used the model during its evolutionary phase have contributed valuable comments and complaints.

NEWS ON ESO INSTRUMENTATION

The ESO TV Autoguiders

M. DUCHATEAU and M. ZIEBELL, ESO

In February 1985 four new autoguiding systems have been installed at La Silla. The 3.6-m telescope, the CAT, the 2.2-m telescope and the Schmidt got equipped with a system.

They have been used now successfully for one and a half year and we hope that they are not "job killers" but that in the meantime they have been accepted as an improvement of work conditions.

Three main reasons induced us to use low-light-level TV cameras for autoguiding:

1. There were already 5 telescopes at La Silla equipped with TV cameras for manual guiding.
2. An electronic crosshair already existed and by setting several electronic signals for it the development of the autoguiding was simplified.
3. Long experience with manual guiding on the Schmidt telescope's electronic crosshair encouraged us to continue in the same direction. The stability of the deflection system of the TV camera did not create any difficulty.

The idea was therefore to use the video signal of a TV camera in connec-

tion with an electronic crosshair as shown in Figure 1:

Except for the TV camera, all the components are installed inside the control consoles. In some locations, the digital memory used for scan conversion in case of an integration facility does not exist. The video signal is then connected directly from the TV camera to the autoguiding chassis (Fig. 2). The advantage of this solution is that no

mechanical and no optical modifications are needed in the focal plane.

Electronic Crosshair

The electronic crosshair, developed to perform corrections for differential refraction on the Schmidt telescope, produces on the monitor one fixed cross, one movable and a rectangular box around the centre of the movable cross-

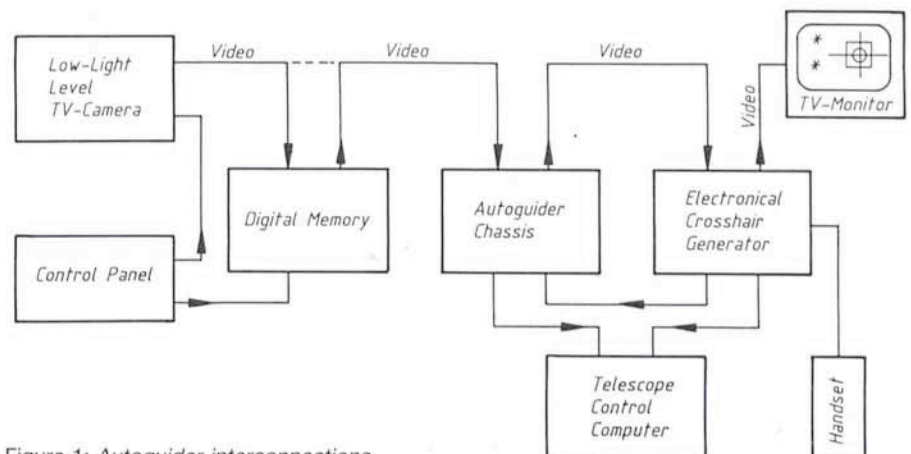


Figure 1: Autoguiding interconnections.

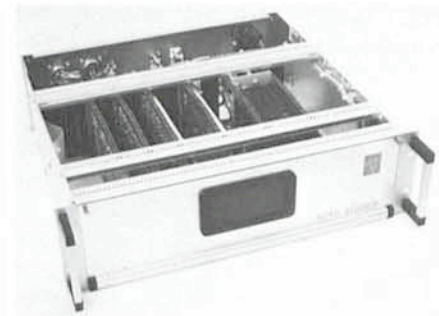


Figure 2: Autoguider.

hair accordingly. In manual guide mode the observer has to follow with his guide star the movable crosshair by correcting the telescope position. With special software the movable crosshair can be used (and it is used so on the Schmidt telescope) for comet tracking.

All the delays which are necessary to build up the cross are produced digitally and do not suffer from temperature effects. The size of the box is adjustable by a handset to fit it to the apparent star diameter under different seeing conditions. The movable crosshair and the box create 4 quadrants. The video signal inside each of these quadrants is integrated and the equilibrium between the four fields is used for autoguiding. All the digital signals for the box (beginning, middle and end in horizontal and vertical direction) are provided by the crosshair and connected to the autoguider.

Autoguider

The basic principle of the autoguider is shown in Figure 5.

Corresponding to the 4 quadrants on the monitor created by the electronic box and the movable crosshair, 4 digital integrators are used to integrate the light over the surface of each quadrant and over an adjustable number of frames. The digital integrator is built out of a 32 bit full adder and a 32 bit register. Each of the registers I_1 , I_2 , I_3 and I_4 is in reality built up out of 2 registers (I and II). Registers I and II contain in principle the same information, register I is just used to produce a short delay before

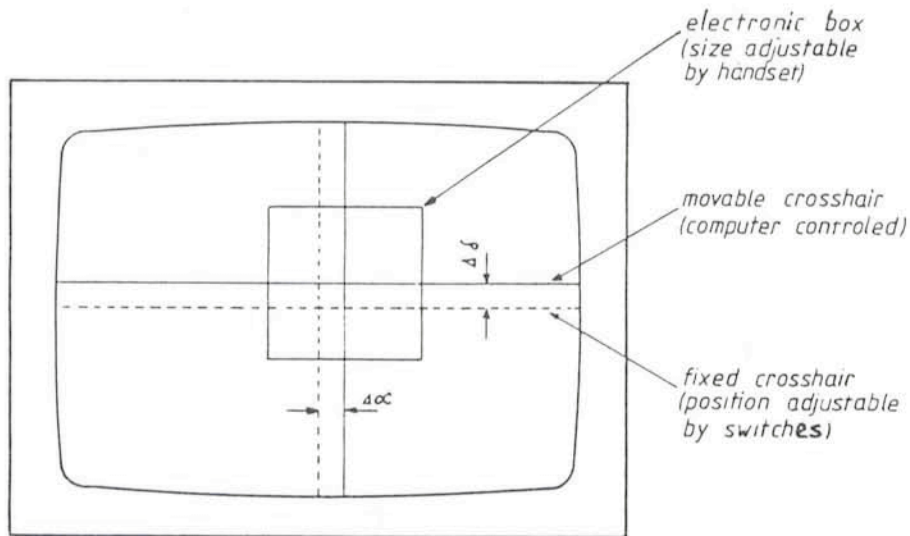


Figure 4.

the information appears at the output of register II. One full adder is commonly used by the 4 channels. After a new conversion of the A/D converter the digital output is transferred via S2 to the full adder and added to the former value which was stored in register II and is now memorized in register I with a certain delay. The new sum is transferred to register II and can be added to the next pixel value. The complete cycle of A/D conversion, integration and transfer to the register takes less than 200 ns. To be more or less independent on different TV cameras, on different black levels (influenced by sky background illumination) and on different dc levels, a special signal clamp has been added in front of the A/D converter. Driven by the switch logic (controller) a Sample & Hold amplifier memorizes the actual analogue voltage of the video signal when the readout beam of the TV-camera passes

into the quadrants at the left side. This analogue voltage is then used as a reference for the A/D converter. This method ensures that only the star light inside the 4 quadrants is integrated with no additional DC level. It makes the autoguider very sensitive and allows automatic guiding on very faint objects. At the 2.2-m telescope stars down to 19th magnitude have been used for autoguiding when using the Boller & Chivens spectrograph. Figure 6a illustrates one TV line which passes through the upper left and upper right quadrant in combination with the modulation signals for the electronic crosshair.

A flag appears on the controller board at the end of the integration time, which can be chosen in a number of frames with a thumb wheel switch behind the front panel. The computer is continuously scanning this bit and when it recognizes "end of integration" it reads the

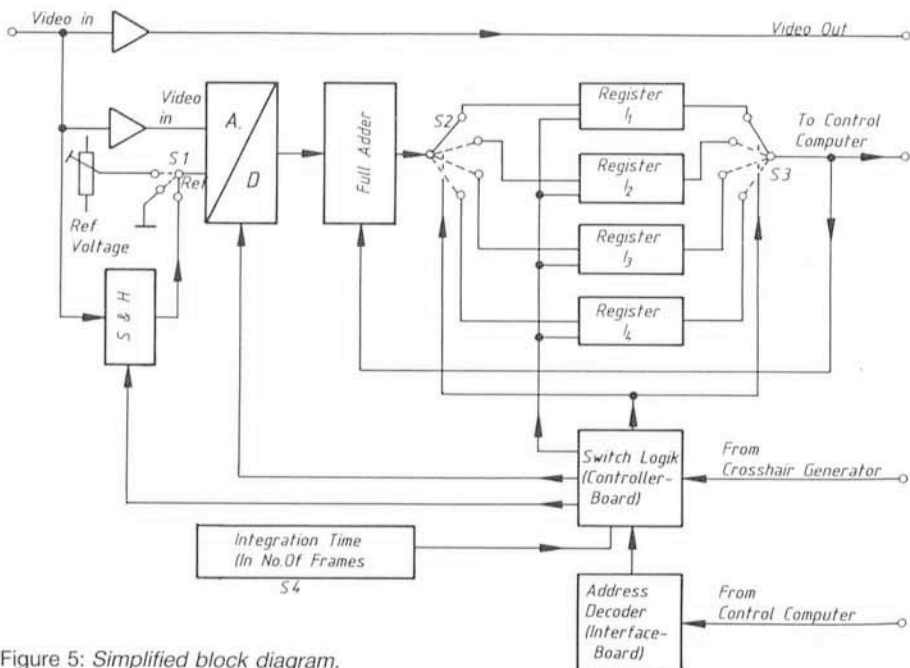


Figure 5: Simplified block diagram.



Figure 3: Crosshair generator.

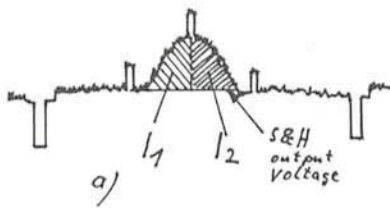
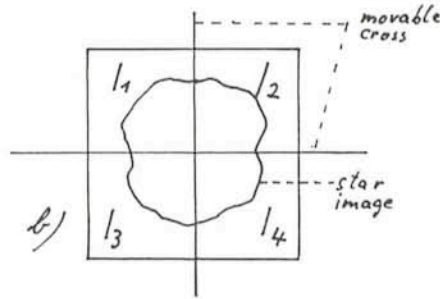


Figure 6a and b.

four integrated values. The address decoding is done on the interface board. When the computer has read the last address all the registers are cleared and a new integration starts automatically.

In the computer the position error is calculated and normalized by:



$$E_x = \frac{I_1 + I_3 - I_2 - I_4}{I_1 + I_2 + I_3 + I_4}$$

$$E_y = \frac{I_1 + I_2 - I_3 - I_4}{I_1 + I_2 + I_3 + I_4}$$

(See Fig. 6b)

The normalization makes the error independent on star magnitudes, seeing

effects and HV adjustments of the TV cameras. To keep the servos of the main drive axis of the telescope stable, an additional measure is to avoid an error proportional speed correction. If an error is detected the corrections will be done by constant offset steps in the right direction.

If the normalized error is bigger than 0.15 then an offset step of 0.1 second of arc is applied. If the error is bigger than 0.85 the offset step will be 0.5 second of arc, but this value can be adjusted depending on optical scales and seeing conditions. For an optical scale of 2.5 lines per second of arc the appropriate step size would be 0.3. If the error is smaller than 0.15 no correction will be applied.

ESO Infrared Specklegraph

C. PERRIER, Observatoire de Lyon, France

Introduction

An infrared specklegraph is available for Visiting Astronomers for use at the 3.6-m telescope F/35 focus. It has briefly been described in the Announcement for Applications in periods 36 to 38. First tested in September 1984, it has since then achieved the expected performances during several runs. However, its theoretical limits have actually been reached only after a dome air-cooling system has been put into operation early this year. In this article we introduce the instrument assuming that the reader already has some knowledge of the short-exposure imaging principles.

The system is based on the slit-scanning technique which allows to obtain one-dimensional images, that is profiles of a source projected onto the scanning direction axis. It aims first of all to diffraction-limited observations; therefore, it is designed for a data rate fast enough to acquire images under conditions of quasi-frozen seeing, and for a spatial sampling adapted to the near-infrared range. The data are stored in the form of individual scans and the data reduction basically yields coadded scans and 1-D visibilities, i.e. Fourier transforms of the source intensity distribution. These visibilities can then be used either directly for size measurements using assumed intensity distribution models or as input to image restoration algorithms.

Instrument Concept

A dedicated dewar equipped with a set of slits and an electronic chain providing a good frequency response is

mounted at the F/35 focus on the infrared photometer adaptor (for a description see Moorwood and van Dijk, *The Messenger*, No. 39, p. 1). The secondary mirror is used to sweep the beam onto the slit and for that purpose is driven with a saw-tooth waveform. During each sweep equally-spaced measures of the flux integrated along the slit are acquired, forming a 1-D image or scan. Rotating the photometer and secondary mirror adaptors gives access to any given position angle (PA).

The requirements have led to an instrument that is a good compromise between good sensitivity in a wide electric bandpass and the specific constraints imposed by the standard infrared instrumental framework. Its current characteristics are shown in Table 1. The system has been optimized for use at L and contains slits adapted to the telescope cut-off frequencies at K, L

and M, plus a wide one for medium-resolution imaging. The maximum data rate well matches the less good conditions under which it is still feasible to obtain high-resolution data down to 2 μ m: atmospheric correlation time ≥ 20 ms and seeing at $V \leq 3$ arcsec. Conversely, the scan time and amplitude may be continuously adjusted up to values sufficiently large to benefit from excellent conditions occurring when the seeing varies slowly. The full resolution of the 3.6-m telescope cannot be achieved at J and H because the usual observing conditions would be too demanding in terms of frequency response; however, it is of course feasible to observe at these wavelengths with the resolution for K.

Part of the acquisition chain is common to both speckle and photometric set-up; this insures some useful standardization. On the contrary, they do not

TABLE 1: SPECKLEGRAPH CHARACTERISTICS

Filters:	wide-band: CVF:	J H K LA M 2.43–4.48 μ m; 4.26–5.32 μ m; resol. $\sim 1/70$
Apertures:	diaphragm \varnothing : slit width:	1.5 4.0 10. arcsec. (saturate at M) 0.105 0.159 0.221 arcsec. (5 arcsec. high) 0.156 0.246 0.464 arcsec. (10 arcsec. high)
Optics:		F/35; linear beam
Detector:	type: frequency response:	Cincinnati hybrid InSb; – G Ω feedback 0.8 @ 100 Hz; 0.4 @ 500 Hz
Electronics:	input range: dynamics:	± 2.5 V after ± 9 V offset & $\times 1-1024$ amplification 4096 ADC units
Scanning:	wave-form: amplitude:	saw-tooth linearity < 1% in useful part 0–40 arcsec. (for 128 pts)
Sampling:		128 or 256 pts/scan; half for source; half for sky 20–600 ms/scan (for 128 pts)
Cryogenics:	outer can: inner can:	liquid N ₂ ; 6–12 h hold time solid N ₂ (55–60 K); > 1–2 weeks hold time